

Investigating opioid vulnerability profiles through a spatial Kalman filter: insights from social and environmental factors

Andrew Deas

Department of Mathematics
University of Tennessee
Knoxville, USA
M.S.

Hashan Fernando

The Bredeesen Center for Interdisciplinary Research
and Graduate Education
University of Tennessee
Knoxville, USA
M.Sc.

Jodie Trafton

Office of Mental Health and Suicide Prevention
Veterans Health Administration
Palo Alto, USA
Ph.D.

Anuj J Kapadia

Computational Sciences and Engineering Division
Oak Ridge National Laboratory
Oak Ridge, USA
Ph.D.

Adam Spannaus

Computational Sciences and Engineering Division
Oak Ridge National Laboratory
Oak Ridge, USA
Ph.D.

Vasileios Maroulas

Corresponding Author
Department of Mathematics
University of Tennessee
202 Ayres Hall
1403 Circle Dr
Knoxville, TN 37916, USA
vmaroula@utk.edu
(865) 974-4302

Keywords: Opioid epidemic, Kalman filter, heat maps, hotspot identification

Word count: 3,619

Abstract

Objective: This study investigates the national opioid crisis by exploring three key social and environmental drivers: opioid-related mortality rates, opioid prescription dispensing rates, and disability rank ordered rates. We introduce a spatial Kalman filter to examine each factor individually and their potential intra-relationships.

Material and Methods: This study utilizes county level data, spanning the years 2014 through 2020, on the rates of opioid-related mortality, opioid prescription dispensing, and disability. To successfully estimate and predict trends in these opioid-related socioenvironmental factors, we augment the Kalman Filter with a novel spatial component. Through this construction we analyze opioid vulnerability at the national scale, creating heat maps and a hotspot analysis.

Results: Our spatial Kalman filter demonstrates strong predictive performance. These predictions are used to uncover pronounced vulnerability profiles for both the rates of opioid-related mortality and disability, finding that the Appalachian region is likely the nation's most vulnerable area to these two factors. This contrasts with a chaotic vulnerability profile found for the dispensing rates.

Discussion: We suggest that the rates of opioid-related mortality and disability are connected and propose that this connection is unlikely to be found in the realm of prescription opioids. Our analysis indicates that prescription opioids are not the primary drivers of opioid-related deaths across the country.

Conclusion: We advocate for comprehensive solutions which extend beyond limiting prescription opioids.

Abstract word Count: 217

BACKGROUND AND SIGNIFICANCE

Propelled by prescription practices and subsequent misuse of opioids, the United States continues to struggle with the opioid crisis.[1–3] The crisis was ignited in the 1990s with the aggressive prescribing of potent opioids like OxyContin. Despite the potential for dependency and abuse, these drugs were marketed with the promise of being non-addictive which led to an increase in prescription opioid consumption and significantly contributed to the epidemic’s progression.[1–3] As the crisis continues to unfold, the medical community and regulatory bodies face the difficult task of balancing effective chronic pain management against the risks of prescription opioid misuse.[4–6] Measures have been implemented to find this balance and curb the spread of opioids;[7] but the evolving landscape of this public health crisis necessitates a continued investigation into the role of prescription opioids.[8,9]

OBJECTIVE

Our study surveys the national opioid crisis by exploring three key social and environmental drivers. In particular, we investigate: opioid-related mortality rates, opioid prescription dispensing rates, and disability rank ordered rates. Each individual factor and their potential intra-relationships is investigated. These factors were chosen for two primary reasons: (1) although efforts have been made to slow down prescription practices, national opioid-related mortality rates are still on the rise;[10] and (2) previous research has suggested that people with disabilities are more likely than the general population to misuse opioids and develop an opioid use disorder.[11]

This investigation leverages a spatial Kalman filter to detail national opioid vulnerability profiles. To define opioid vulnerability, we used heat maps of the distribution of rates across the nation’s counties and identified the hotspots. In this context, hotspots are defined on a year-by-year basis as counties with rates in the top 5% nationally. Multiple contiguous hotspot counties are referred to as clusters of hotspots and indicate the most vulnerable areas in the nation.

For data estimation and prediction, the cornerstone of this analysis utilizes a spatial Kalman filter. The Kalman filter, frequently used in temporal statistical modeling, traditionally lacks a spatial framework.[12, 13] However, in our study we augment the Kalman filter with a spatial component. This spatial component is designed to capture the complex geographical interrelations among counties within the United State’s diverse landscape, thereby improving the accuracy of our opioid-related data estimations and predictions.

This study utilizes rates of opioid-related mortality, opioid prescription dispensing, and disability aggregated at the county level spanning the years 2014 through 2020. The final year in the study represents the latest point of comprehensive data collection across the datasets; but also stands as a pivotal moment in public health due to the COVID-19 pandemic. Although the impact of COVID-19 on the opioid crisis and its disruption of data collection are outside the scope of this study,

it is important to acknowledge that the challenges associated with the opioid crisis were notably exacerbated by the 2020 pandemic.[14–17] Consequently, 2020 is a critical year for examination within the context of the opioid crisis.

This paper begins by framing our study within the scope of existing research, followed by a detailed exposition of the data and methodologies employed. We then articulate our findings before delving into a discussion that situates these findings within the wider discourse on managing the opioid crisis. We conclude by highlighting this study’s implications for future research directions and public health strategies.

Related Works

The intertwined dynamics of opioid mortality, prescription rates, and social vulnerability has been explored in previous research.[18–20] Such studies have concluded that the crisis’s roots extend beyond prescription practices to broader socioenvironmental issues and advocate for addressing structural addiction determinants.[7,21] In particular, social vulnerability factors such as disability, population density, and minority status have been identified as significant predictors of drug overdose mortality.[22] Building upon such previous insights, our study offers novel geospatial evidence to the discussion.

The Kalman filter uses a series of observations to estimate unknown parameters and has been applied in many diverse settings from navigating astronauts to the moon to real-time vehicle tracking.[12, 13, 23, 24] In such Kalman filter applications, numerous methods have been innovated to integrate spatial components into the filter.[25–28] For example, one study integrated the Kalman filter with the Kriging method; while another utilized the Kalman filter in conjunction with a separate spatiotemporal model. Extending this line of innovation, our study incorporates a spatial component through the process covariance matrix. Within this matrix, an exponential decay function is used to model spatial correlations. Our novel and independently derived approach bears similarity to the one adopted by Rougier et al.[29] in 2022; they however utilized an alternative function to compute covariance.

Heat maps are widely recognized and utilized for their efficacy in visualizing data intensity across regions. They translate complex datasets into choropleth maps. These maps facilitate an intuitive grasp of the varied vulnerability levels across a geographical landscape.[30] To further delineate such landscapes, hotspot identification is frequently used. Its utilization can play a pivotal role in epidemiology and public health research for pinpointing areas that are disproportionately impacted by various health issues.[31–34] For example, advanced Bayesian models have identified Ohio’s most vulnerable hotspots to opioid overdose mortality,[35] and spacetime random forest models have unraveled the complex geospatial patterns of opioid-related crime in Chicago.[36] Our study highlights the public health utility of integrating the Kalman filter with both heat maps and hotspot identification.

MATERIALS AND METHODS

Data

This study examines the rates of opioid-related mortality, opioid prescription dispensing, and disability across the United States from 2014 to 2020. It is important to note that each dataset was collected differently: the opioid-related mortality rates are measured per 100,000 persons, the opioid prescription dispensing rates are measured per 100 persons, and the disability rank ordered rates are measured as percentile ranks from 0 to 100. Throughout our study period, there were adjustments to the national county landscape, such as the formation of new counties and the reconfiguration of existing ones.[37] Our data has been carefully curated to reflect the county structure as of 2020 (in which there are 3143 counties). This step ensures that we provide the most up-to-date and cohesive representation of the national county landscape with respect to the data.

If annual data rates were missing for certain counties, we assigned a value of 0 to those counties. This approach was chosen over data imputation because some counties were missing data for the inaugural year of 2014. Additionally, each dataset had different sets of missing counties and time periods, so assigning missing values to 0 provided a consistent method to handle missing data across all datasets. In this way, counties with missing data were effectively excluded, thus preventing their potential bias in the overall findings.

The drug mortality data were sourced from HepVu, originally collected by the Centers for Disease Control and Prevention’s (CDC) National Center for Health Statistics and the National Vital Statistics System.[38] These data represent narcotic overdose deaths per 100,000 persons, classified according to the International Classification of Diseases, Tenth Revision (ICD-10) codes.[39] It is important to understand that these rates serve as indicators of opioid misuse rather than exact counts of opioid overdose mortality. Also sourced from the CDC are the opioid dispensing rates; these data reflect the rates of retail opioid prescriptions dispensed per 100 persons per year.[40]

The disability rates utilized in this study are measured as percentile rank estimates of the civilian non-institutionalized population with a disability in each county. These data were sourced from the CDC and Agency for Toxic Substances and Disease Registry’s Social Vulnerability Index (SVI) which utilizes data from the American Community Survey to assess the resilience of communities to external stresses on human health.[41] Given the SVI’s biennial publication, we impute data for the intervening years by calculating half the difference between consecutive biennial data points and adding it to the earlier year’s rates. This method, with the understanding that yearly rate fluctuations are modest, provided a viable way to analyze the impact of disability rank ordered rates on the national opioid crisis throughout the entire study period. Notably, Rio Arriba County, New Mexico, experienced a data collection error in 2018.[42] Therefore, for this county, we employed a more granular approach by taking a quarter of the difference between the 2016 and 2020 data points and adding it consecutively to each year starting in 2016.

Kalman filter model

The trajectory of the opioid crisis inherently contains both geospatial and temporal dimensions. The temporal dimension contains the details of the crisis’s evolution over time. This temporal evolution can be leveraged to uncover patterns and trends which provide a deeper understanding of the epidemic. On the other hand, the information contained in the geospatial dimension is the spatial distribution and clustering of opioid-related variables. This spatial information can be utilized to highlight geographical disparities and identify localized areas of concern. Consequently, to successfully estimate and predict trends in opioid-related socioenvironmental factors, our model assimilates both the geospatial and temporal dimensions.

Our framework analyzes opioid trajectories in the United States at the county-level and treats the state of the nation in any given year t as a random vector, $N_t \in \mathbb{R}^d$, where d is the number of counties in the nation. The nation is modeled as evolving from its immediate past state, N_{t-1} , by the following equation:

$$N_t = N_{t-1} + \varepsilon_t, \quad \varepsilon_t \sim \mathcal{N}(0, Q). \quad (1)$$

The normal random vector ε_t represents the change in the nation’s state from one year to the next.

The process covariance matrix Q is specifically designed to capture the spatial correlations between counties. The entries of $Q = [q_{ij}]$ are inversely proportional to their respective county’s geographical centers of population [43] x_i and x_j , computed through an exponential decay function:

$$q_{ij} = \exp\{-b \cdot d(x_i, x_j)\}.$$

Here q_{ij} denotes the correlation between two counties, $d(x_i, x_j)$ represents the geographical distance between x_i and x_j measured using the haversine function, and $b > 0$ is the decay rate that modulates the speed at which correlation decreases with distance. This decay rate is tailored to each factor in the data independently; and ensures that the correlation q_{ij} diminishes to 50% at a predetermined distance threshold. This threshold is derived from the approximate diameter of the most visually pronounced vulnerable region identified in the heat map visualizations of the data. In this way, we ensure a higher correlation among proximate counties and a significantly reduced correlation for more distant ones. Further details on the parameter values utilized in our study are available in the Python code which constructs the covariance matrices for each dataset. This code can be found in the Github repository linked in the supplementary materials section.

Our observed data, i.e., the rates of opioid-related mortality, prescriptions and disability in year t , can be modeled, with some degree of error, as measurements of the true underlying state. Thus, letting D_t symbolize the observed data for an opioid-related variable in year t , the observation can be modeled as:

$$D_t = N_t + \eta_t, \quad \eta_t \sim \mathcal{N}(0, R). \quad (2)$$

The normal random vector η_t represents the measurement error in data collection, reporting, or other discrepancies from the true state. R is the observation covariance matrix and quantifies the uncertainty in the data measurements. To choose a data uncertainty level for our study, we conducted a sensitivity analysis. This analysis examined various uncertainty levels, specifically 1%, 3%, and 5%, by evaluating the respective changes in the model’s predictive performance. Optimal predictive accuracy was found with a 1% data uncertainty level. Consequently, a 1% uncertainty assumption was adopted for all data measurements throughout our study. The results of this sensitivity analysis are summarized in Appendix A.

Our framework of the dynamics driving the opioid crisis is aligned with the operational principles of the Kalman filter. The Kalman filter operates on the foundation of two principal equations: the state update equation and the observation equation. The state update equation delineates the evolution of the system’s state from one time point to the next; while the observation equation connects the true state of the system to the measurements or observed data. Together these equations form the core mechanics of the Kalman filter and enable it to accurately estimate a system’s state by updating previous predictions with new observational data.

We utilized the Kalman filter to model opioid crisis dynamics by selecting eq. (1) as the filter’s state update equation and eq. (2) as the filter’s observation equation. This choice allowed a smooth integration of the temporal dimension of opioid-related data by capitalizing on the Kalman filter’s inherent temporal nature. Additionally, the spatial dimension was woven into the analysis through the covariance matrix Q in eq. (1). This matrix was specifically designed to capture spatial correlations between counties. For a rigorous mathematical exposition of the Kalman filter algorithm, see Appendix B, and for further reading, see [12] and [13].

RESULTS

Efficacy of opioid-related data predictions

Presented here are the results for our spatial Kalman filter which was initialized with 2014 data and trained on data from 2015 to 2019 before generating predictions for 2020. Training, in this context, means allowing the filter to refine its estimates using the observed data; while its estimates were made without further refinement in the 2020 prediction year. We chose to predict for only a single year to prevent the accumulation of large errors inherent in multi-year forecasting. Long-term forecasting is accommodated by the filter’s design however, and investigated in Appendix D. In this investigation, the efficacy of multi-year predictions from the filter is examined by comparing its performance when trained on progressively less data to that of the fully trained filter discussed here. Presented in this section are the efficacy results for the filter’s 2020 predictions. For the remaining years in the study, the efficacy metrics are summarized in Appendix C. In addition, the corresponding accuracy maps and error histograms can be found in the supplementary materials.

The efficacy of our spatial Kalman filter in predicting county-level rates is quantitatively assessed using both accuracy and error metrics on a national scale. The accuracy metric results are visualized using accuracy maps; while error histograms are used to display the results of the error metrics. The metric used to calculate the error for each county is the absolute residual. The largest absolute residual, stemming from the filter’s worst annual prediction, is then used to assess general accuracy in the following way: each county’s error is normalized by the highest annual error observed nationwide. In addition to general accuracy, we also compute hotspot accuracy. Hotspots are defined on a year-by-year basis as counties with rates in the top 5% nationally. The number of hotspots correctly predicted by the filter divided by the number of actual hotspots is defined as the hotspot accuracy.

For opioid-related mortality rates, measured per 100,000 persons, the filter achieved an average general accuracy of 93.62%. The national accuracy distribution is displayed in Figure 1a. This map is characterized predominantly by green hues, indicating high predictive accuracy across the nation. A distinct region of lower accuracy, marked by yellow and red hues, is found in the southern part of West Virginia. This region experienced significant jumps in mortality rates from 2019 to 2020. These large jumps were difficult for the filter to predict and led to these distinguishable errors. The range of errors for this dataset, shown in fig. 2a, illustrates that our model’s mortality rate estimates can deviate from the actual rates by an average of 5.57 deaths per 100,000 persons, with a maximum deviation of 87.27 deaths per 100,000 persons in the worst case. Additionally, for this dataset, the filter achieved a hotspot accuracy of 71.50%. The hotspots which were correctly identified and those that were missed are shown in fig. 3a.

For the disability rank ordered rates, measured as percentile ranks from 0 to 100, our spatial Kalman filter demonstrated excellent predictive performance. The range of errors, shown in fig. 2b, demonstrates that our model’s disability rank ordered rate estimates can deviate from the actual rank ordered rates by an average of 1.57 percentile rank points, with a maximum deviation of 15.85 percentile rank points in the worst case. This efficacy of the filter is also highlighted by its high

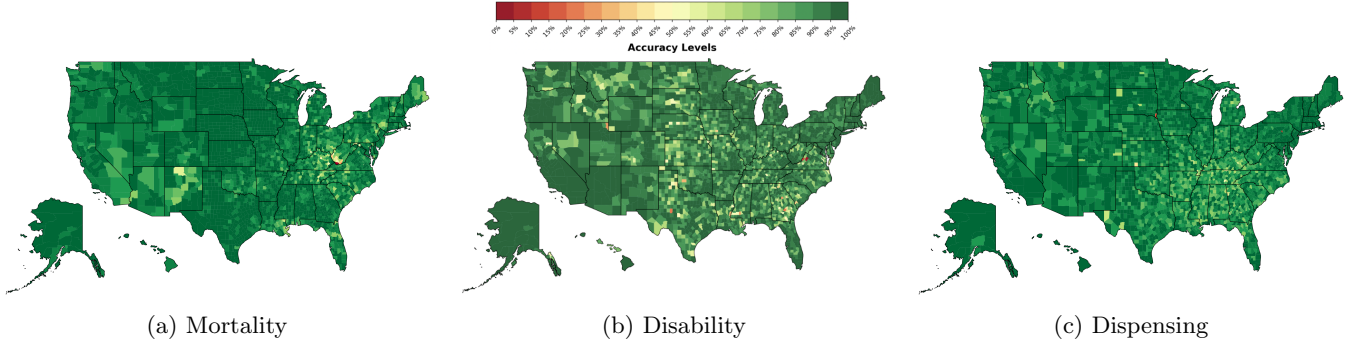


Figure 1: General accuracy maps for the 2020 (a) mortality, (b) disability, and (c) dispensing rate predictions. The maps are color-coded to represent increasing intervals of accuracy by 5%, starting from dark red for the least accurate predictions, and progressing to dark green for the most accurate predictions.

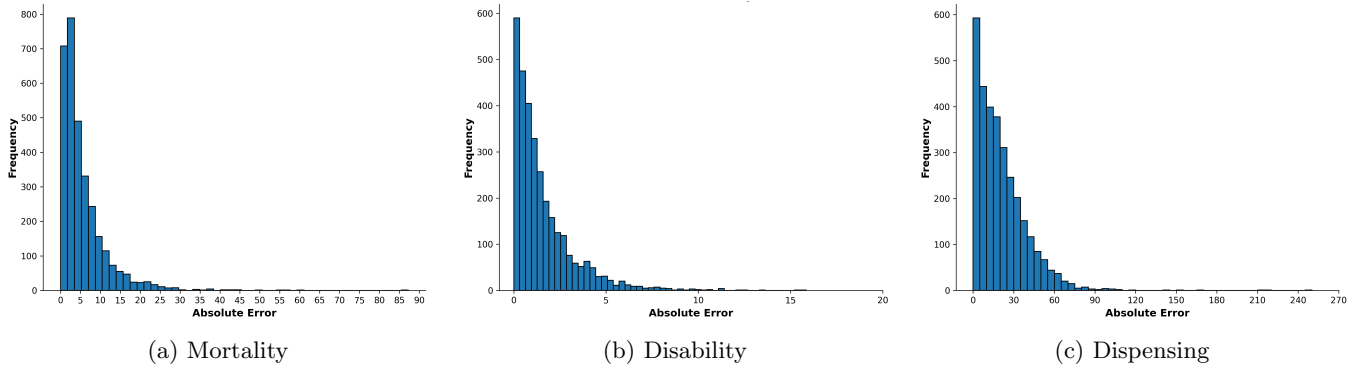


Figure 2: Histograms displaying the distribution of the filter’s absolute errors for the 2020 (a) mortality, (b) disability, and (c) dispensing rate predictions.

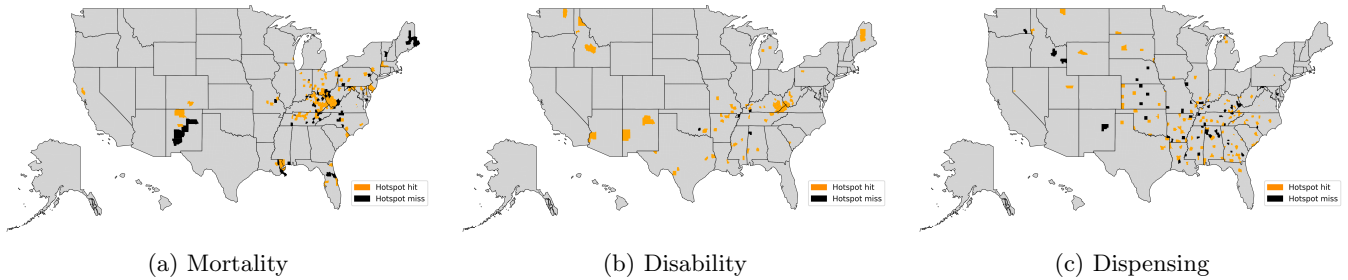


Figure 3: Hotspot accuracy maps for the 2020 (a) mortality, (b) disability, and (c) dispensing rate predictions. Orange colored counties represent accurately predicted hotspots, whereas those in black mark hotspots missed by our predictions.

hotspot accuracy of 95.35%. The correctly predicted hotspots and those that were missed are shown in fig. 3b. On the other hand, the average general accuracy score of 90.08% may not fully convey the filter’s effectiveness on this dataset. This is because the maximum annual error of 15.85 used for normalization on this dataset results in even relatively small errors appearing more pronounced. This is visually evident in fig. 1b; where we observe more yellow tones, denoting this magnification of smaller errors.

For the prescription dispensing rates, measured per 100 persons, the filter’s predictions attained an average general accuracy of 91.69%. The national accuracy distribution is visualized in fig. 1c. This map is predominantly green; but upon close inspection, two red counties stand out: Union, South Dakota, and Montour, Pennsylvania. These counties experienced an extraordinary increase of over 350% in their dispensing rates from 2018 to 2019. Based on this surge, the filter predicted similarly high increases from 2019 to 2020. However, the increases in 2020 were far less dramatic, leading to these significant prediction errors. The range of errors for this dataset, shown in Figure 2c, illustrates that our model’s dispensing rate estimates can deviate from the actual dispensing rates by an average of 20.81 prescriptions per 100 persons, with a maximum deviation of 250.27 prescriptions per 100 persons in the worst case. Additionally, the filter’s hotspot accuracy on this dataset was 68.05%. The correctly identified hotspots and those that were missed are shown in fig. 3c.

Predicted vulnerability profiles

Presented here are the results of leveraging our spatial Kalman filter to detail national opioid vulnerability profiles. This is done by constructing heat maps of the distribution of rates across the nation’s counties and identifying the hotspots. To this end, the filter’s normal distributions in each year are utilized to calculate the cumulative distribution function values for each county. These values are then used to categorize the counties into 20 distinct vulnerability levels in intervals of 5 percentile each. This results in a color gradient on the heat maps, transitioning from dark blue for the least vulnerable counties with the lowest rates to dark red for the most vulnerable counties with the highest rates. The most vulnerable counties, i.e., the counties whose predicted rates surpass the 95th percentile of the fitted normal distributions, are identified on a year-by-year basis and defined as the hotspots. Multiple contiguous hotspot counties are referred to as clusters of hotspots and indicate the most vulnerable areas in the nation. The results presented in this section are for the filter’s predictions in 2020, the results for the remaining years in the study period can be found in the supplementary materials.

The vulnerability profile for the opioid-related mortality rates uncovered by our spatial Kalman filter is displayed in fig. 4a. In this profile, widespread vulnerability is found with pronounced differences between regions. In the Northern and Southern regions, there are pockets of lower mortality rates, suggesting resilience. In contrast, pronounced vulnerability is exhibited in the Eastern and Western regions. Within these regions, the Appalachian area, i.e., encompassing Ohio, Kentucky, West Virginia, Virginia, and Tennessee, emerges as a critical area of concern. Additionally, this region contains the most visually evident cluster of hotspots. This is seen in fig. 5a, and means that the most vulnerable counties in the nation, with respect to opioid-related mortality rates, are primarily found within the Appalachian region.

The vulnerability profile for the disability rank ordered rates revealed by our filter is shown in fig. 4b. In this profile, the North and West regions display notably lower rates of disability,

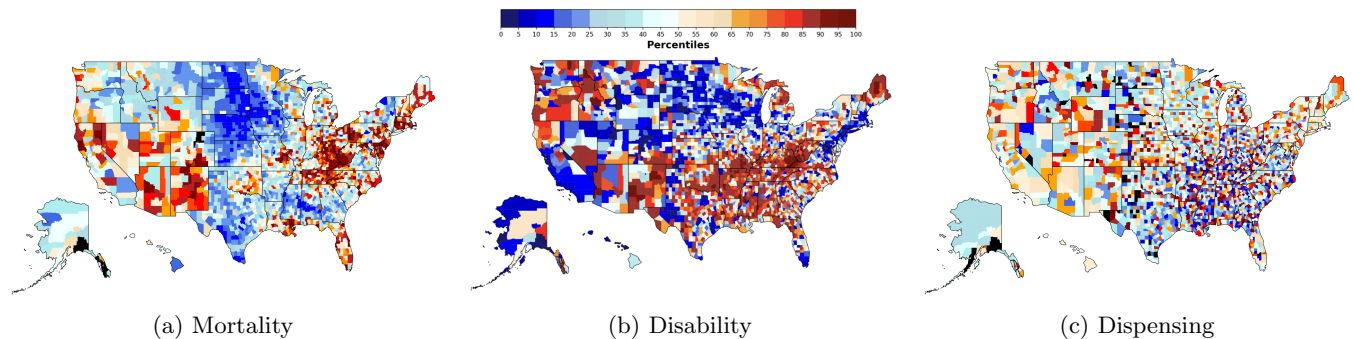


Figure 4: Heat maps for the 2020 (a) mortality, (b) disability, and (c) dispensing rate predictions. The maps are color-coded to represent increasing levels of vulnerability by 5th percentiles, starting with dark blue for the counties with the lowest rates, and progressing to dark red for the counties with the highest rates. Counties with missing data are colored in black.

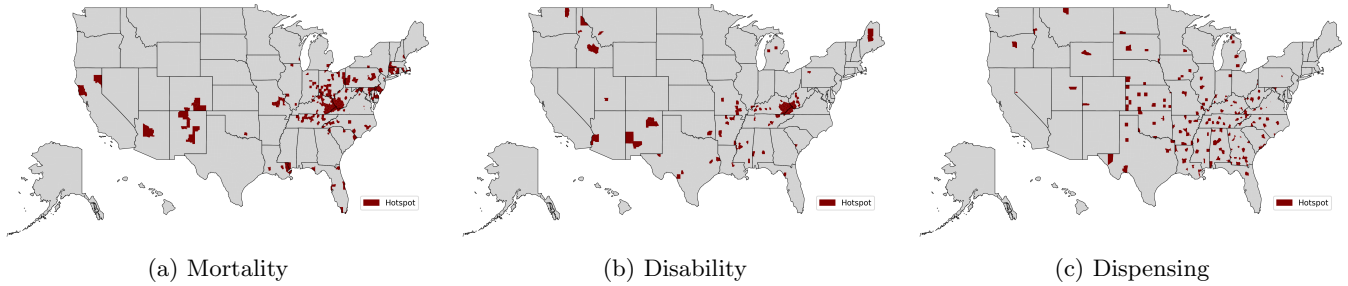


Figure 5: Hotspot maps for the 2020 (a) mortality, (b) disability, and (c) dispensing rate predictions. These maps highlight the counties whose rates exceed the 95th percentile of the fitted normal distribution, categorizing them as having the highest vulnerability level.

indicating regions of relative resilience. In contrast, significant vulnerable areas are found primarily in the South, Northwest, and Appalachian regions. Within these regions, the hotspots are dispersed, as seen in fig. 5b. This maps shows that the Appalachian region contains the most visually evident cluster of hotspots once again; strongly suggesting that this region not only contains the nation’s most vulnerable counties with respect to opioid-related mortality rates, but also with respect to the disability rank ordered rates.

The vulnerability profile for prescription dispensing rates uncovered by our filter is shown in fig. 4c. In this map, lower rates nationwide are predominantly observed, indicating the nation’s state is one of greater resilience than vulnerability. However, this profile exhibits a notably chaotic pattern which, for the most part, lacks coherent clusters of both resilience and vulnerability. Yet, although there are small pockets of contiguous resilient and vulnerable counties distributed throughout the nation, these pockets are far less visually pronounced than those observed in the previous two vulnerability profiles. Additionally, as seen in fig. 5c, the hotspots are erratically spread across the nation with no visually noteworthy clusters of contiguous hotspot counties.

DISCUSSION

The predictions of our spatial Kalman filter provided insights into the 2020 national opioid crisis vulnerability profiles of three factors: opioid-related mortality rates, opioid-dispensing rates, and disability rank ordered rates. The analysis of the mortality rates revealed a widespread national vulnerability profile where the Appalachian region was distinguished as the nation’s most vulnerable area to opioid-related mortality. Correspondingly, the analysis examining the disability rank ordered rates also uncovered a widespread vulnerability profile where the Appalachian region, due to its most visually pronounced cluster of hotspots, was once again pinpointed as the nation’s most vulnerable area to disability rank ordered rates. This dual identification of the Appalachian region as the nation’s most vulnerable area to both mortality and disability rates suggests that amidst the general fabric of the opioid crisis, these two factors may share a critical link. This potential connection echoes previous findings,[7, 22, 44] underscores the disproportionate outcomes of the opioid crisis

and highlights the pressing need for support in the Appalachian region.

Contrasting sharply with the patterns observed for the mortality and disability rates, our filter’s predictions for the prescription dispensing rates revealed a chaotic vulnerability profile. This profile did not have any visually discernible spatial patterns, lacked notable clusters of hotspots, and generally exhibited more resilience than vulnerability across the nation. When juxtaposed against the other considered factors, this more resilient characteristic suggests that difficulties with opioid prescription practices are dispersed and not restricted to localized areas. That said, this resilience also implies that current prescription practices may not be the immediate focal point of concern. In fact, the lack of alignment between the vulnerability profiles of prescription and mortality rates indicates that prescription opioids might not be the primary drivers of opioid-related fatalities nationwide. A conclusion that aligns with previous research,[7, 21] and is additionally bolstered by contrasting national trends observed during our study period: despite a sharp 52.84% drop in dispensing rates from 2014 to 2020, opioid mortality surged by 73.73%.

The distinct differences between the vulnerability profile for prescription rates and the profiles for both mortality and disability rates suggest a nuanced insight: it is unlikely that prescription opioids are the link between mortality and disability rates; rather, it is more plausibly found in the realm of illicit drug use or other complex factors. This insight underscores the intricacies of the opioid crisis and highlights the need for comprehensive solutions that go beyond merely reducing opioid prescriptions. Multifaceted and nuanced strategies which address the broader spectrum of contributing factors is what our research advocates for.

CONCLUSION

Our study uncovered a potential connection between disability and opioid-related mortality rates but no clear link with prescription opioids. This invites future research to explore or discount additional variables, such as other social vulnerability factors, that might elucidate or rule out the nature of the relationship between these two factors. The possible link between them was found through the dual identification of the Appalachia region as the nation’s primary area of concern for both mortality and disability rates. Future research could investigate the unique policies and practices in the Appalachian region to dissect the roots of its pronounced vulnerability.

Additionally, this study showcased our spatial Kalman filter’s exceptional ability to predict outcomes in spatially oriented datasets. The methodologies outlined in this study could be adapted and enhanced by future research to explore a wide spectrum of phenomena or challenges embedded within both the spatial and temporal dimensions. Additionally, subsequent research could also harness the filter’s potential for long-term forecasting to predict outcomes over extended periods of time. Finally, given the overlap of our study’s time frame with the COVID-19 pandemic, future research could explore the impact of the 2020 pandemic on the rates of opioid-related mortality, opioid prescriptions, disability, and their interrelations.

ACKNOWLEDGEMENTS

This work is sponsored by the US Department of Veterans Affairs using resources from the Knowledge Discovery Infrastructure which is located at the Oak Ridge National Laboratory and supported by the Office of Science of the U.S. Department of Energy. This manuscript has been authored by UT-Battelle, LLC, under contract DE-AC05-00OR22725 with the US Department of Energy (DOE). The US government retains and the publisher, by accepting the article for publication, acknowledges that the US government retains a nonexclusive, paid-up, irrevocable, worldwide license to publish or reproduce the published form of this manuscript, or allow others to do so, for US government purposes. DOE will provide public access to these results of federally sponsored research in accordance with the DOE Public Access Plan (<http://energy.gov/downloads/doe-public-access-plan>)

The authors would like to thank Heidi A Hanson and Andrew Farrell for their helpful comments and feedback, not only on the manuscript, but throughout the entire study.

In this study, ChatGPT-4 served as an alternative to traditional online search tools, such as Google and StackExchange. Additionally, it provided guidance on optimizing the geographic representation of Alaska and Hawaii in the map generation code utilized in our analyses.

COMPETING INTERESTS

The authors have no competing interests to declare.

AUTHOR CONTRIBUTIONS

AD curated the data, generated the code, and wrote the initial manuscript. AS conceptualized the overall research project and provided general oversight and expertise. VM proposed the use of the Kalman filter for prediction, supervised the detailed execution of the project and provided methodological expertise. All authors reviewed the manuscript and contributed to revisions.

SUPPLEMENTARY MATERIALS

The code and data required to replicate our work is provided at: <https://github.com/A-Deas/Hotspots.git>

APPENDIX

A. Data uncertainty level sensitivity analysis

B. The Kalman filter algorithm

We present a mathematical exposition of the Kalman filter algorithm. The Kalman filter estimates a system's state over time through prediction and update phases. In the prediction phase,

Data Uncertainty Level	Mortality	Disability	Dispensing
1% uncertainty	93.62%	95.35%	91.69%
3% uncertainty	93.45%	88.92%	90.03%
5% uncertainty	93.37%	88.64%	89.03%

Table 1: Average general accuracy for the filter’s 2020 mortality, disability and dispensing rate predictions as the level of uncertainty in the data increases. The most significant drop in accuracy is observed in the disability rates dataset. The narrow range and tight clustering of these percentile ranks between 0 and 100 each year, combined with the use of synthetic data for intervening years, make this dataset particularly sensitive to increased uncertainty, due to a broader range of estimations from the filter.

the current state, $\hat{N}_{t|t-1}$, and error covariance matrix, $P_{t|t-1}$, are forecast based on the previous state and error covariance matrix as follows:

$$\begin{aligned}\hat{N}_{t|t-1} &= F_t \hat{N}_{t-1|t-1} \\ P_{t|t-1} &= F_t P_{t-1|t-1} F_t^\top + Q_t.\end{aligned}$$

We set the matrix Q_t to the covariance matrix Q in eq. (1) for all t , which encapsulates the spatial relations in the data defined in eq. (2). The matrix F_t models the system dynamics, taken to be the identity matrix for all t as our model assumes a linear progression of the system state over time.

During the update phase, upon receiving the annual data D_t , the filter refines its estimates using a weighted average term, K_t , called the Kalman gain. The Kalman gain is calculated to adjust predictions based these new measurements, subsequently updating the current state estimate $\hat{N}_{t|t}$ and error covariance matrix $P_{t|t}$ as follows:

$$\begin{aligned}K_t &= P_{t|t-1} H_t^\top (H_t P_{t|t-1} H_t^\top + R_t)^{-1} \\ \hat{N}_{t|t} &= \hat{N}_{t|t-1} + K_t (D_t - H_t \hat{N}_{t|t-1}) \\ P_{t|t} &= (I - K_t H_t) P_{t|t-1}.\end{aligned}$$

H_t is the measurement model, taken to be the identity matrix in order to directly identify counties with their data. R_t is the measurement noise covariance matrix, set to the identity matrix scaled by 0.01 to reflect the assumed 1% uncertainty in the data measurements.

C. Efficacy summary for the spatial Kalman filter during training years

We provide the details of the Kalman filter’s efficacy in estimating the rates of mortality, prescriptions, and disability across the training years in the study period. Excluding the initialization year of 2014, the subsequent training years, 2015 to 2019, are pivotal for the filter’s learning phase, where its estimates are refined using the observed data. The output for these years therefore consists of calibrated estimates which showcase the filter’s evolution as it iteratively learns underlying trends in the data. In table 2, we provide the efficacy metric results for each dataset and each

training year.

Variable	Year	Avg General Acc	Hotspot Acc	Avg Error	Max Error
Mortality rates	2015	96.58%	97.31%	0.31	9.07
	2016	94.57%	96.55%	0.37	6.84
	2017	94.21%	95.54%	0.40	6.98
	2018	94.55%	94.34%	0.38	6.90
	2019	93.87%	95.0%	0.38	6.14
Disability rates	2015	92.26%	99.38%	0.58	7.49
	2016	91.75%	98.82%	0.77	9.33
	2017	92.06%	99.41%	0.72	9.06
	2018	92.73%	98.82%	0.86	11.80
	2019	91.31%	97.59%	0.81	9.30
Dispensing rates	2015	96.47%	91.49%	0.46	13.15
	2016	96.05%	87.36%	0.55	13.98
	2017	96.53%	95.45%	0.46	13.26
	2018	97.99%	91.86%	0.46	22.97
	2019	97.50%	93.81%	1.81	72.28

Table 2: Efficacy metric results for the Kalman filter during the 2015 to 2019 training years

D. Multi-year predictive efficacy of the spatial Kalman filter

Our study optimized the Kalman filter’s predictive accuracy by using all five available training years from 2015 to 2019, then forecasting only for 2020. However, the filter is capable of making predictions over multiple years. Here we explore the multi-year predictive efficacy of the filter by training it with progressively less data, decreasing from four training years down to just one, then extending the prediction periods accordingly. For example, the filter trained on a single year of data, is initialized with 2014 data, learns from 2015 data then generates predictions for the years 2016 through 2020. This approach allowed us to assess the impact of training length on prediction accuracy over extended forecasting horizons.

Figure 6 showcases a comparative histogram analysis of the filter’s errors for the year 2020 when it is trained on progressively less data versus the fully trained filter. Since errors steadily accumulate for each consecutive prediction year, we showcase the results for 2020 to offer a clear view of the filter’s performance degradation as it is trained on less data. The histogram comparisons for the remaining years in the study can be found in the supplemental materials.

As expected, training the filter on less data leads to an incremental increase in both the frequency of errors and the magnitude of the maximum error, the latter of which is highlighted by a red arrow in each histogram. As the training period shortens for mortality and dispensing rates, we note an increase in maximum errors and the error distributions shifting rightward. Despite this, considering the limited data it had to learn from, the filter still maintains a commendable performance on these datasets.

However, the biennial publication of disability rates, coupled with our method of synthesizing

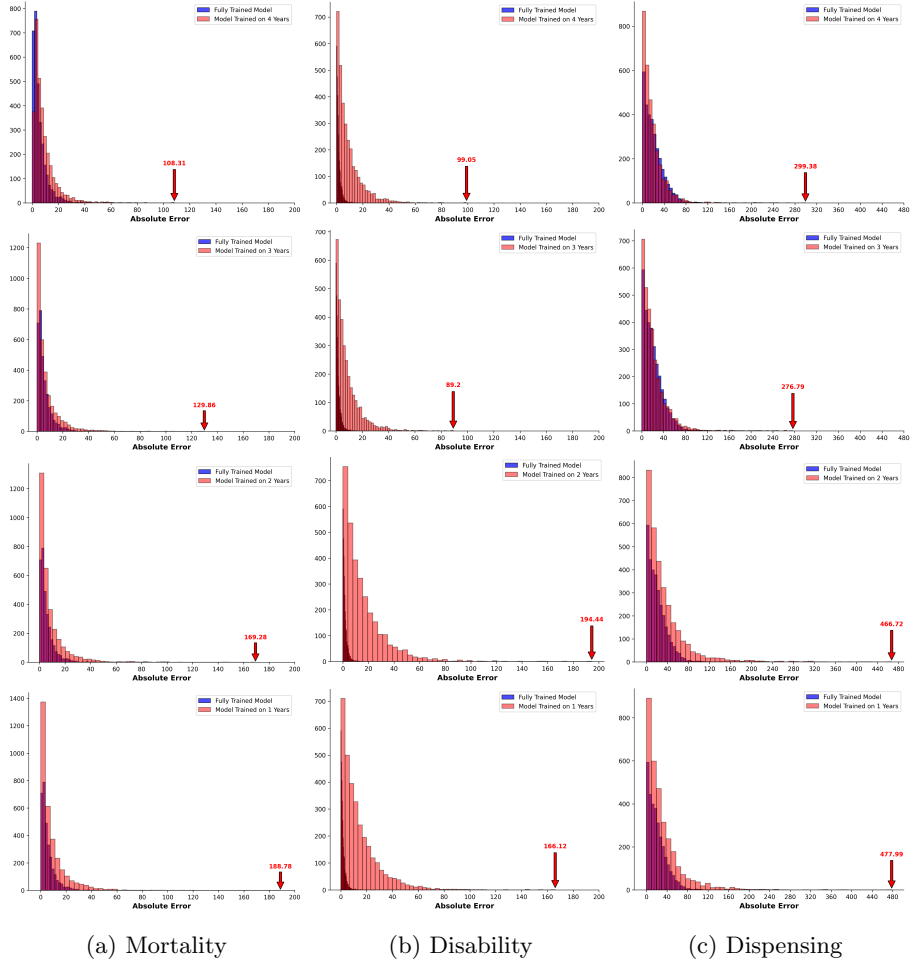


Figure 6: Histogram comparisons of the absolute errors for the 2020 (a) mortality, (b) disability, and (c) dispensing rate predictions between the fully trained filter and the filter trained on progressively less data. The error distribution of the fully trained filter is colored in blue, whereas the error distribution of the filter trained on less data is colored in red. The top row showcases comparisons for the filter trained on four years of data, iteratively progressing downwards to the last row showcasing comparisons for the filter trained on a single year of data. Each histogram features a red arrow highlighting the maximum error from the filter trained on less data.

the intervening annual data, poses distinct challenges for multi-year disability rate predictions. Specifically, this data structure causes the filter to mistakenly extrapolate trends over two-year periods, leading to considerable errors in its multi-year predictions. Such issues become intractable in the absence of intervening data points and result in the filter failing to properly adjust its projections. This problem is evident in fig. 6, where the error distributions of the filter trained on less data are notably more extensive and pronounced compared to the fully trained filter. This scenario underscores the critical importance of consistent annual data collection to sustain the filter’s predictive accuracy across longer forecasting intervals.

REFERENCES

- [1] Manchikanti L, Atluri S, Hansen H, et al. Opioids in chronic noncancer pain: have we reached a boiling point yet? *Pain Physician* 2014;17(1):E1-10.
- [2] Ciccarone D. The triple wave epidemic: Supply and demand drivers of the US opioid overdose crisis. *Int J Drug Policy* 2019;71:183-188.
- [3] Centers for Disease Control and Prevention. Understanding the Opioid Overdose Epidemic. 2023. <https://www.cdc.gov/opioids/basics/epidemic.html>. Accessed January 3, 2024.
- [4] Dong X, Deng J, Rashidian S, et al. Identifying risk of opioid use disorder for patients taking opioid medications with deep learning. *J Am Med Inform Assoc* 2021;28(8):1683–1693.
- [5] Singh N, Varshney U. Adaptive interventions for opioid prescription management and consumption monitoring. *J Am Med Inform Assoc* 2023;30(3):511–528.
- [6] Chrianna B, Hickman M, Barbieri S, et al. Big data and predictive modelling for the opioid crisis: existing research and future potential. *Lancet Digit Health* 2021;3(6):E397-E407.
- [7] Judd D, King CR, Galke C. The Opioid Epidemic: A Review of the Contributing Factors, Negative Consequences, and Best Practices. *Cureus* 2023;15(7): e41621.
- [8] Guy Jr GP, Zhang K, Bohm MK, et al. Vital Signs: Changes in Opioid Prescribing in the United States, 2006–2015. *MMWR Morb Mortal Wkly Rep* 2017;66(26):697-704.
- [9] McElfresh DC, Chen L, Oliva E, et al. A call for better validation of opioid overdose risk algorithms. *J Am Med Inform Assoc* 2023;30(10):1741–1746
- [10] National Institute on Drug Abuse. Drug Overdose Death Rates, Figure 4. 2023. <https://nida.nih.gov/research-topics/trends-statistics/overdose-death-rates#:~:text=Drug%20overdose%20deaths%20involving%20prescription,involving%20prescription%20opioids%20totalled%2016%2C706..> Accessed February 15, 2024.

- [11] National Institute on Disability, Independent Living, and Rehabilitation Research at Administration for Community Living. Summary of Responses from a Request for Information: People with Disabilities and Opioid Use Disorder. 2020. <https://acl.gov/news-and-events/announcements/summary-responses-request-information-people-disabilities-and-opioid>. Accessed February 15, 2024.
- [12] Kalman RE. A New Approach to Linear Filtering and Prediction Problems. *J Fluids Eng* 1960;82(1):35-45.
- [13] Meinhold RJ, Singpurwalla ND. Understanding the Kalman Filter. *Am Stat* 1983;37(2):123-127.
- [14] Knoebel RW, Kim SJ. Impact of COVID-19 Pandemic, Social Vulnerability, and Opioid Overdoses in Chicago. *AJPM Focus* 2023;2(2):100086.
- [15] Xia Z, Stewart K. A counterfactual analysis of opioid-involved deaths during the COVID-19 pandemic using a spatiotemporal random forest modeling approach. *Health Place* 2023;80:102986.
- [16] Holmes LM, King BH. County-level variation in synthetic opioid and heroin overdose incidents in Pennsylvania during the COVID-19 pandemic. *Applied Geography* 2023;155:102977.
- [17] King B, Holmes LM, Rishworth A, et al. Geographic variations in opioid overdose patterns in Pennsylvania during the COVID-19 pandemic. *Health Place* 2023;79:102938.
- [18] Grigoras CA, Karanika S, Velmahos E, et al. Correlation of Opioid Mortality with Prescriptions and Social Determinants: A Cross-sectional Study of Medicare Enrollees. *Drugs* 2018;78(1):111-121.
- [19] Bohnert ASB, Valenstein M, Bair MJ, et al. Association Between Opioid Prescribing Patterns and Opioid Overdose-Related Deaths. *JAMA* 2011;305(13):1315-21.
- [20] Cheattle MD. Prescription Opioid Misuse, Abuse, Morbidity, and Mortality: Balancing Effective Pain Management and Safety. *Pain Med* 2015;16(Suppl 1):S3-S8.
- [21] Dasgupta N, Beletsky L, Ciccarone D. Opioid Crisis: No Easy Fix to Its Social and Economic Determinants. *Am J Public Health* 2018;108(2):182-186.
- [22] Tatar M, Faraji MR, Keyes K, et al. Social vulnerability predictors of drug poisoning mortality: A machine learning analysis in the United States. *Am J Addict* 2023;32(6):539-546.
- [23] Jack Trainer. How NASA Used the Kalman Filter in the Apollo Program. <https://www.lancaster.ac.uk/stor-i-student-sites/jack-trainer/how-nasa-used-the-kalman-filter-in-the-apollo-program>. Accessed October 7, 2023.

- [24] Lim CH, Ong LY, Lim TS, et al. Kalman Filtering and Its Real-Time Applications [Internet]. Real-time Systems. InTech 2016. <http://dx.doi.org/10.5772/62352>.
- [25] Mardia K, Goodall C, Redfern E, et al. The Kriged Kalman Filter. *TEST: An Official Journal of the Spanish Society of Statistics and Operations Research* 1998;7:217-282.
- [26] Huang HC, Cressie N. Spatio-temporal prediction of snow water equivalent using the Kalman filter. *Comput Stat Data Anal* 1996;22(2):159-175.
- [27] Wikle CK, Cressie N. A Dimension-Reduced Approach to Space-Time Kalman Filtering. *Biometrika* 1999;86(4):815-829.
- [28] Achar A, Bharathi D, Kumar BA, et al. Bus Arrival Time Prediction: A Spatial Kalman Filter Approach. *IEEE trans Intell Transp Syst* 2020;21:1298-1307.
- [29] Rougier J, Brady A, Bamber J, et al. The scope of the Kalman filter for spatio-temporal applications in environmental science. *Environmetrics* 2023;34(1):e2773.
- [30] Gehlenborg N, Wong B. Heat maps. *Nat Methods* 2012;9(3):213.
- [31] Lessler J, Azman AS, McKay HS, et al. What is a Hotspot Anyway? *Am J Trop Med Hyg* 2017;96(6):1270-1273.
- [32] Stopka TJ, Krawczyk C, Gradziel P, et al. Use of Spatial Epidemiology and Hot Spot Analysis to Target Women Eligible for Prenatal Women, Infants, and Children Services. *Am J Public Health* 2014;104(Suppl 1):S183–S189.
- [33] Shariati M, Mesgari T, Kasraee M, et al. Spatiotemporal analysis and hotspots detection of COVID-19 using geographic information system (March and April, 2020). *J Environ Health Sci Eng* 2020;18(2):1499–1507.
- [34] Stopka TJ, Laroche MR, Li X, et al. Opioid-related mortality: Dynamic temporal and spatial trends by drug type and demographic subpopulations, Massachusetts, 2005–2021. *Drug Alcohol Depend* 2023;246:109836.
- [35] Hernandez A, Branscum AJ, Li J, et al. Epidemiological and geospatial profile of the prescription opioid crisis in Ohio, United States. *Sci Rep* 2020;10:4341.
- [36] Xia Z, Stewart K, Fan J. Incorporating space and time into random forest models for analyzing geospatial patterns of drug-related crime incidents in a major U.S. metropolitan area. *Comput Environ Urban Syst* 2021;87:101599.
- [37] United States Census Bureau. Table & Geography Changes. 2024. <https://www.census.gov/programs-surveys/acs/technical-documentation/table-and-geography-changes.2022.html#list-tab-71983198>. Accessed October 19, 2023.

- [38] Hepvu. Tools & Resources. 2024. <https://hepvu.org/resources/#/additional-data>. Accessed October 19, 2023.
- [39] Hepvu. Data Methods. 2024. <https://hepvu.org/data-methods/>. Accessed October 19, 2023.
- [40] Centers for Disease Control and Prevention. United States Dispensing Rate Maps. 2023. <https://www.cdc.gov/drugoverdose/rxrate-maps/index.html>. Accessed October 17, 2023.
- [41] Centers for Disease Control and Prevention/Agency for Toxic Substances and Disease Registry. CDC/ATSDR SVI Data and Documentation Download. 2022. https://www.atsdr.cdc.gov/placeandhealth/svi/data_documentation_download.html. Accessed October 13, 2023.
- [42] United States Census Bureau. Data Collection Error in Rio Arriba County, NM. 2020. <https://www.census.gov/programs-surveys/acs/technical-documentation/errata/125.html>. Accessed February 15, 2024.
- [43] United States Census Bureau. Centers of Population. 2021. <https://www.census.gov/geographies/reference-files/time-series/geo/centers-population.html>. Accessed January 29, 2024.
- [44] Schalkoff CA, Lancaster KE, Gaynes BN, et al. The opioid and related drug epidemics in rural Appalachia: A systematic review of populations affected, risk factors, and infectious diseases. *Subst Abus* 2020;41(1):35-69.